Journal of Alloys and Compounds 517 (2012) 69–74

Contents lists available at SciVerse ScienceDirect

Journal of Alloys and Compounds

journal homepage: www.elsevier.com/locate/jallcom

# Functional properties of electrospun NiO/$RuO_2$ composite carbon nanofibers

Yongzhi Wu[a,b,c], Rajiv Balakrishna[a,b], M.V. Reddy[b,*], A. Sreekumaran Nair[a,*], B.V.R. Chowdari[b], S. Ramakrishna[a,d]

[a] Healthcare and Energy Materials Laboratory, Nanoscience and Nanotechnology Initiative, National University of Singapore, Singapore 117576, Singapore
[b] Physics Department, National University of Singapore, Singapore 117542, Singapore
[c] NUS Graduate School for Integrated Science & Engineering, 10 Kent Ridge Crescent, National University of Singapore, Singapore 119260, Singapore
[d] Kind Saud University, Riyadh 11451, Saudi Arabia

ARTICLE INFO

*Article history:*
Received 8 October 2011
Received in revised form 2 December 2011
Accepted 7 December 2011
Available online 17 December 2011

*Keywords:*
Electrospinning
Nanofibers
NiRu–CNF
Supercapacitor
Anode
Lithium batteries

ABSTRACT

One-dimensional (1D) nickel oxide/ruthenium oxide (NiO/$RuO_2$)–carbon composite nanofibers (NiRu–C–NFs) were fabricated via electrospinning of a homogenous mixture of polyacrylonitrile (PAN) and Ni/Ru salt precursors at different ratios followed by heat treatments. The 1D nanostructures of the composite material were characterized by field-emission scanning electron microscopy (FE-SEM), powder X-ray diffraction (XRD), Rietveld refinement and Brunauer–Emmett–Teller (BET) surface area measurements. Li-cycling properties were evaluated using cyclic voltammetry and galvanostatic properties. The asymmetric hybrid supercapacitor studies were carried out with activated carbon as a cathode and NiRu–C–NFs composites as anodes in the cycling range, 0.005–3.0 V using 1 M $LiPF_6$ (EC;DMC) electrolyte. NiRu–C–NFs fabricated from 5 wt% nickel (II) and 15 wt% ruthenium (III) precursors showed a capacitance up to ~60 F $g^{-1}$ after 30 cycles. Anodic Li-cycling studies of NiRu–C–NF-0 and NiRu–C–NF-2 composite samples showed a reversible capacity of 230 and 350 m Ahg$^{-1}$ at current rate of 72 mA $g^{-1}$ at the end of 40th cycle in the voltage range of 0.005–3.0 V. Electrochemical impedance studies (EIS) on NiRu–C–NFs showed lower impedance value for 15 wt% Ru than the bare sample.



## 1. Introduction

The development of supercapacitors and lithium-ion batteries (LIBs) has received a rising attraction devoted to applying either high power or high energy in the latest demands in electric energy storage units for battery powered electric vehicles (EVs) and plug-in hybrid-electric vehicles (HEVs and PHEVs) [1]. Of late, great interests are shown by researches on nanostructures in energy storage systems, due to their relatively higher surface area and shorter diffusion pathway [2–4]. Carbon-based materials are the preferred candidates in electrodes, because of their excellent electronic conductivity, electrochemical stability in different working conditions, high surface areas and low cost. Various carbon forms ranging from allotropes (graphite, fullerenes, nanotubes, and graphene) to different morphologies (foams, fibers and gels) have been tested as electrodes in either supercapacitors or LIBs [5,6]. Carbon based 1D nanostructured composites have been extensively explored to enhance the overall performance with various methods, including chemical vapor deposition (CVD) [7–9] and electrospinning [10–12]. Electrospinning is a simple and cost-effective methodology to mass fabricate continuous ultra-fine nanofibers with high aspect ratios [13,14] and various functional metal oxides, such as electrospun $TiO_2$ [15,16], and $Nb_2O_5$ [17], have found applications as battery materials.

Anodic Li-cycling properties of NiO were first reported by group of Tarascon [18], later electrochemical performance of different morphologies NiO are well studied and summarized in the recent review papers [4,19]. Carbon materials-based nanocomposites with metal oxides such as nickel oxide (NiO) and ruthenium oxide ($RuO_2$) have been identified as electrode material for supercapacitors. NiO has the advantage of abundance and low price while $RuO_2$ is preferred due to its high conductivity and three accessible distinct oxidation states [20] with potential ultrahigh capacitance up to 1000 F $g^{-1}$ [21,22]. Synthesis of composites such as $RuO_2$–CNFs [23] and NiO–CNFs [11] has been reported in recent years and found to have unique morphology and high specific capacitance individually. However, to the best of our knowledge, the combination of the three components: NiO, $RuO_2$, and CNF, has not been reported yet.

In this work, NiO/$RuO_2$–CNFs were fabricated in the application of both asymmetric supercapacitors and anodic Li-cycling studied

* Corresponding authors. Tel.: +65 6516 2956; fax: +65 6777 6126.
*E-mail addresses:* phymvv@nus.edu.sg (M.V. Reddy), nniansn@nus.edu.sg (A.S. Nair).

0925-8388/$ – see front matter © 2011 Elsevier B.V. All rights reserved.
doi:10.1016/j.jallcom.2011.12.019

in the range, 0.005–3.0 vs. $Li/Li^+$. The electrospun nanocomposites have been structurally and texturally characterized by different techniques.

## 2. Experimental

### 2.1. Synthesis of nickel/ruthenium–carbon composite nanofibers

Nickel acetate tetrahydrate (purity 99%, Aldrich) and ruthenium acetylacetonate (RuAcAc) (purity 99%, Aldrich) were mixed with 10 wt% polyacrylonitrile (PAN, Aldrich) polymer in *N*,*N*-dimethyl-formamide (DMF, Aldrich 99%). Typically, three different solutions were prepared separately by maintaining the wt% of nickel acetate tetrahydrate at 5 wt% while the wt% of RuAcAc was varied from 0, 5, 15 wt% in the 10 wt% solution of PAN (in DMF). The corresponding materials were denoted as NiRu–C–NF-0, NiRu–C–NF-1, NiRu–C–NF-2, respectively. The solution was stirred for 24 h using a magnetic stirrer to ensure homogeneity of the solution. Electrospinning was carried out using a commercial machine, NANON (MECC, Japan) under an applied voltage of 30 kV, with G 28 1 1/2 stainless steel needle. The humidity level inside the electrospinning chamber was ~50%. The flow rate of the spinning solution was set to 1 mL/h while the distance between the collector plate and the syringe needle tip was around 15 cm. The as-spun fibers were collected on an alumina foil in the form of a freestanding membrane and were stabilized in air atmosphere at 280 °C for 1 h to retain nanofiber structures. Carbonization process was conducted by sintering the stabilized material at 800 °C for 1 h in presence of Argon to obtain the final nanocomposites. Detailed nanostructure of NiRu–C–NF nanocomposites was characterized by scanning electron microscopy (SEM, JEOL JSM-6700F), X-ray diffractometer (XRD, Xpert MPD PANalytical) and BET studies (NOVA 4200E Surface Area and Pore Size Analyzer, Quantachrome, USA).

### 2.2. Electrochemical characterization

For electrochemical studies, electrodes were fabricated by mixing the active material, super carbon black and binder (polyvinylidene difluoride, PVDF) in the weight ratio: 70:15:15 using *N*-methyl pyrrolidone (NMP) as solvent to dissolve the PVDF binder. The mixture was uniformly spread on an etched copper foil (thickness, 15 μm) with thickness of 10 μm as current collector by using a doctor-blade technique and dried at 80 °C under vacuum. The activated carbon (AC) (BET surface area 880 (±20) $m^2\,g^{-1}$, Norit, The Netherlands) electrode was prepared with 80 wt% AC, 10 wt% super P carbon, and 10 wt% binder coated on Cu-foil. Then the electrodes were pressed using stainless steel (SS)-roller, was cut into 16 mm thick circular disks. The coin-cells (size 2016; 20 mm diameter and 1.6 mm thick) were fabricated inside an Argon-filled glove box (MBraun, Germany) which maintains <1 ppm of $H_2O$ and $O_2$. Active carbon (AC) electrode and lithium metal foil (Kyokuto metal Co., Japan) served as counter electrodes in supercapacitor and anodic Li-cycling studies, respectively. Electrolyte used was 1 M $LiPF_6$ in ethylene carbonate (EC)–diethyl carbonate (DEC) (1:1 in volume) (Merck) mixture for both supercapacitor and Li-cycling studies. Celgard 2502 membrane was used as the separator. The cells were aged for 24 h before measurement. More details on electrode fabrication discussed in previous studies [24,25]. Charge–discharge cycling tests and corresponding kinetic studies were performed at a constant current mode between 0.005 and 3 V vs. $Li/Li^+$ using a computer controlled Bitrode battery tester (Model SCN-12-4-5/18, USA). Several current densities were tried. Impedance spectra were measured on cells using a Solartron impedance/gain-phase analyzer (model SI 1255) coupled with a potentiostat (SI 1268) at room temperature. The frequency ranged from 0.18 MHz to 36 mHz with an ac signal amplitude of 10 mV. Further details on instrumentation are reported in previous studies [26].

## 3. Results and discussion

### 3.1. Structure and morphology

The SEM images of electrospun nanofibers (NiRu–C–NF-0, NiRu–C–NF-1, NiRu–C–NF-2) after carbonization at 800 °C for 1 h share similar characters of smooth and uniform surfaces with occasional bead-like structures indicating the presence of attached metal oxides (Fig. 1a–c). There is no significant difference in the diameters of nanofibers among the three different loadings (Table 1). As could be seen, the long duration and high temperature of the carbonization process spoil the fiber morphology but increase graphite crystallization as shown in previous studies [27,28]. Our results could be taken as a reasonable outcome of a short-term sintering time at 800 °C.

Fig. 2a shows the results of X-ray diffraction (XRD) measurement of NiRu–C–NF-0 (5% Ni) obtained after calcination process.

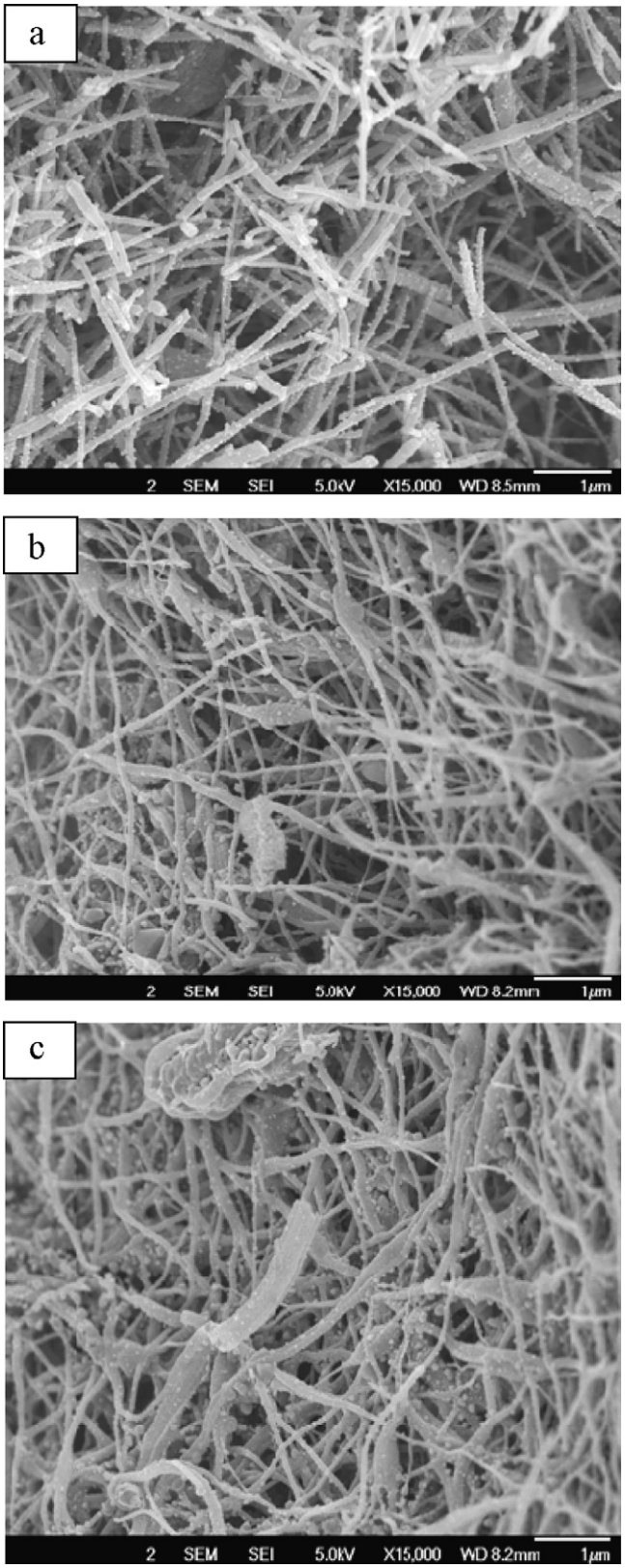


**Fig. 1.** SEM images of the electrospun nanofibers after the carbonization process: (a) NiRu–C–NF-0 (5% Ni); (b) NiRu–C–NF-1 (5% Ni, 5% Ru); and (c) NiRu–C–NF-2 (5% Ni, 15% Ru), respectively.

Rietveld refinement of the as-received XRD patterns indicates the presence of embedded Ni particles in the CNFs. The three broad diffraction peaks shown at $2\theta = 44^\circ$, $52^\circ$ and $76^\circ$, respectively, were assigned to a typical Ni (FCC) structure. This was due to the fact that during carbonization process, the small amount of nickel precursors would be reduced to Ni in presence of carbon in inert atmosphere. Similar conclusions could also be drawn from Fig. 2b and c. When the weight percentages of the precursor salts increased, corresponding metal oxides appeared. For NiRu–C–NF-0 (5% Ni), carbon content was enough to reduce most nickel salts. As more salts were added in NiRu–C–NF-1 (5% Ni, 5% Ru), there were less carbon components that could only turned a certain part of nickel salts into Ni. The XRD studies result for NiRu–C–NF-1 showed the only existence for embedded ruthenium while NiRu–C–NF-2 (5% Ni, 15% Ru) had peaks for ruthenium oxide. Further details on space group, lattice parameter values and theoretical density of composite samples were given in Table 1. The lattice parameter and density values obtained using TOPAS software version 2.1. It clearly showed the presence of Ni, Ru and their corresponding oxides on carbon nanofibers.

BET surface area for carbon nanofibers is also shown in Table 1. NiRu–C–NF-0 is observed to have the largest surface area of 182 ($\pm$0.2) $m^2/g$, while NiRu–C–NF-1 and NiRu–C–NF-2 have surface areas of 38 and 66 ($\pm$0.2) $m^2/g$, respectively. The value is much lower than that of the bare CNF [27,29] because of the higher density of the Ni- and Ru oxides-embedded composites. The decrease in surface area for the NiRu–C–NF-1 and NiRu–C–NF-2 from NiRu–C–NF-0 can be expected via the comparison of SEM images (Fig. 1a shows less common bead-like structures than Fig. 1b and c) due to the presence of either ruthenium ions or ruthenium oxides. However, increasing the composition of ruthenium also increases the surface area of the NFs. The mechanism is still unclear to us; yet, such a trend of increasing surface area is preferred in the electrochemical properties.

### 3.2. Anodic electrochemical studies vs. Li

The comparison of the cyclic voltammograms (CV) of NiRu–C–NF-0 and NiRu–C–NF-2 vs. Li in the voltage range, 0.005–3.0 V for selected cycles (1st, 2nd and 5th) is shown in Fig. 3. As can be seen in Fig. 3a, for NiRu–C–NF-0 the initial cathodic scan showed peaks at ~0.74 V and ~1.13 V; the trends in the subsequent scans indicated carbon dominated effects. Other features are: (1) cathodic current was much higher than anodic current; (2) anodic peak shifted to almost 1 V; (3) many moderate peaks exhibited the possible reaction of NiO and carbon phases with lithium. The main cathodic and anodic peak voltages, consistent with previous report [30], confirmed the main structure of metallic nickel deposited on carbon nanofibers. On the contrary, Li insertion and extraction peaks during oxidation and reduction for NiRu–C–NF-2 were much more distinct. The redox peaks during the first cycle located at 0.01 V,

**Table 1**
Fibers diameter, BET surface area and lattice parameter values NiRu–C–NF composites.

| | NiRu–C–NF-0(5% Ni) | NiRu–C–NF-1 (5% Ni, 10% Ru) | NiRu–C–NF-2 (5% Ni, 15% Ru) |
|---|---|---|---|
| Fiber diameter (nm) | 80 | 70 | 80 |
| BET surface area ($m^2/g$) | 181.7 | 38.1 | 65.7 |
| Lattice parameter (Å) | | | |
| Ni | $a$ = 3.521(6) | $a$ = 3.545(0) | $a$ = 3.524(3) |
| NiO | $a$ = 4.173(2) | $a$ = 4.176(7) | $a$ = 4.159(7) |
| Ru | – | $a$ = 2.692(1), $c$ = 4.268(4) | $a$ = 2.690(0), $c$ = 4.258(2) |
| $RuO_2$ | – | – | $a$ = 4.472(2), $c$ = 3.093(3) |
| Space groups | | | |
| Ni | Fm-3m (FCC) | Fm-3m (FCC) | Fm-3m (FCC) |
| NiO | Fm-3m (FCC) | Fm-3m (FCC) | Fm-3m (FCC) |
| Ru | – | P63/mmc (T) | P63/mmc (T) |
| $RuO_2$ | – | – | P42/mnm (T) |
| Calculated theoretical density ($g/cm^3$) from XRD data | | | |
| Ni | 8.93 | 8.74 | 8.91 |
| NiO | 7.55 | 7.34 | 7.63 |
| Ru | – | 12.53 | 12.58 |
| $RuO_2$ | | – | 7.14 |

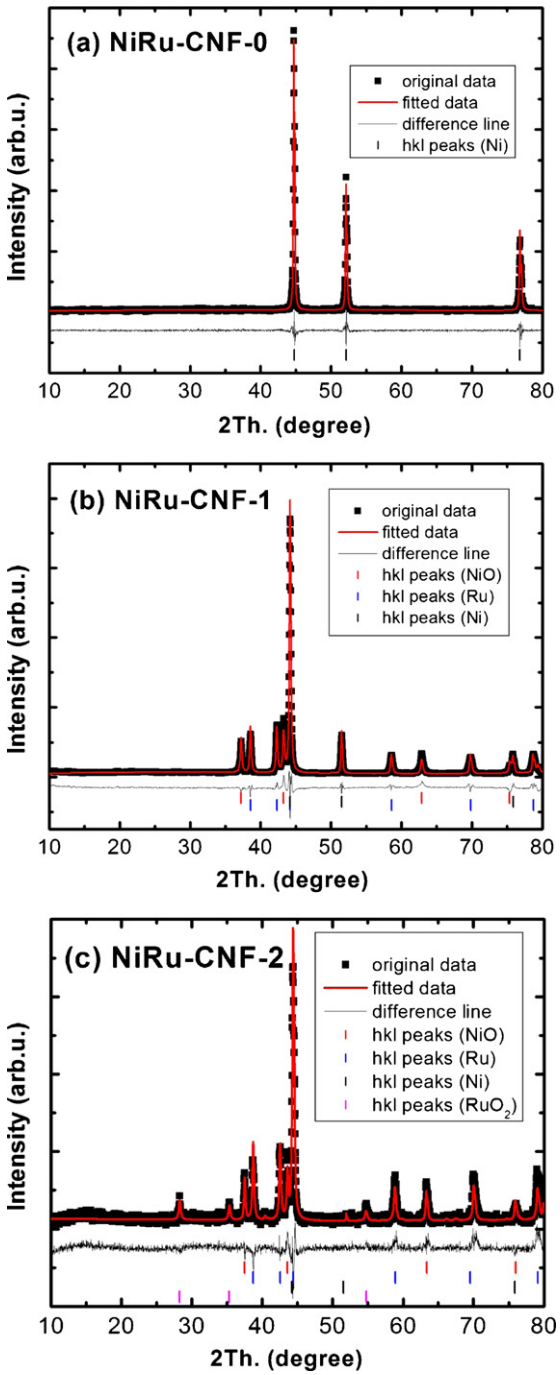


**Fig. 2.** Rietveld refined X-ray diffraction patterns carbon composites with (a) NiRu–C–NF-0 (5% Ni); (b) NiRu–C–NF-1 (5% Ni, 5% Ru); and (c) NiRu–C–NF-2 (5% Ni, 15% Ru).

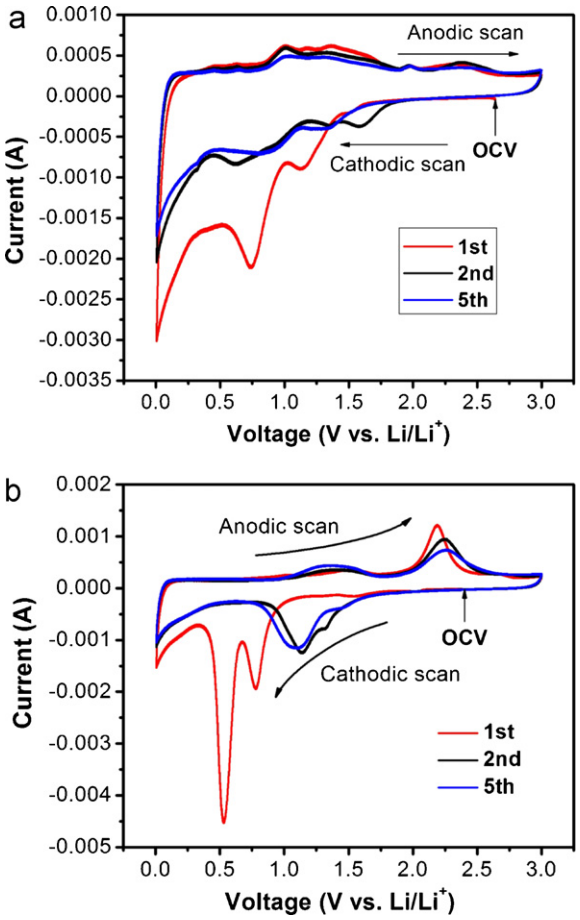


**Fig. 3.** The cyclic voltammograms (CV) of (a) NiRu–C–NF-0 (5% Ni) and (b) NiRu–C–NF-2 (5% Ni, 15% Ru); voltage range, 0.005–3.0 V; scan rate, 0.058 mV/s.

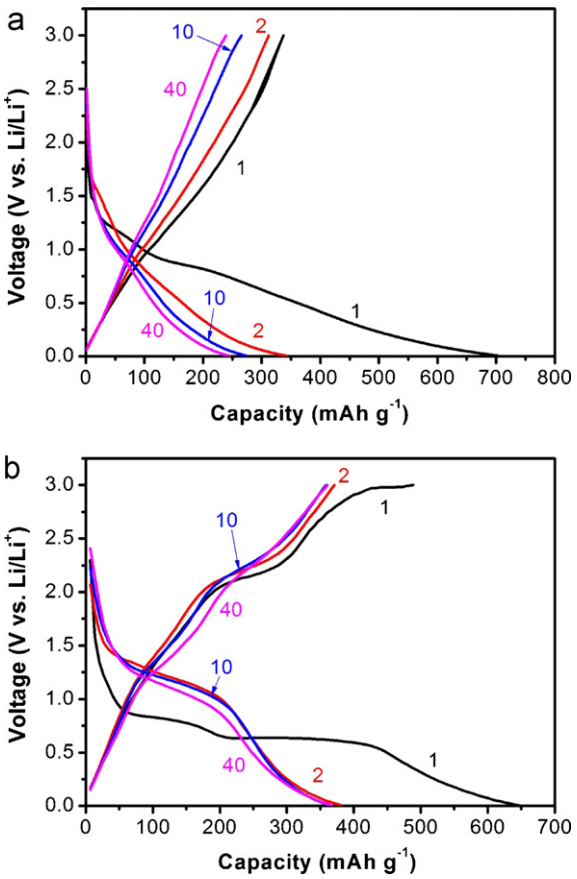


**Fig. 4.** Galvanostatic cycling profiles of (a) cell Li/NiRu–C–NF-0 (5% Ni) and (b) cell Li/NiRu–C–NF-2 (5% Ni, 15% Ru) at 1, 2, 10, and 40th cycle. Voltage range, 0.005–3.0 V; current rate, 72 mA $g^{-1}$.

0.78 V and 0.53 V, respectively, indicating the intercalation/de-intercalation reaction of Li with carbon ($6C + Li^+ + e^- \rightarrow LiC_6$) and NiO ($NiO + 2Li^+ + 2e^- \rightarrow Ni + Li_2O$). A strong peak located at 2.19 V was detected in the first anodic scan, which corresponds to the formation of NiO ($Ni + Li_2O \rightarrow NiO + 2Li^+ + 2e^-$) [31–34]. In the second cathodic/anodic scan, the peaks shifted to 1.14 V and 2.25 V, respectively, owing to the structural rearrangement or the formation cycle during the initial discharge/charge process [33,34]. The trends for peaks shift during subsequent cycles obtained using CV were close to previous studies on graphite or some form of carbon and NiO anode materials [4,31–35]. It was evident that the CV traces of NiRu–C–NF-2 indicated improved performance for Li-insertion and extraction compared to those of NiRu–C–NF-0. There was no sign of Ru or $RuO_2$ in the CV for NiRu–C–NF-2 because their contribution is very limited possibly due to the inactive Ru and the overlap of peaks due to $RuO_2$.

Galvanostatic cycling profiles of Li/NiRu–C–NF-0 and Li/NiRu–C–NF-2 cells were recorded at a constant current density of 72 mA $g^{-1}$ between 0.005 V and 3 V at room temperature. Selected discharge–charge curves of 1, 2, 10, and 40th cycles were shown in Fig. 4a and b, respectively. No distinct voltage plateaus could be observed for cell Li/NiRu–C–NF-0 throughout all the 40 cycles (Fig. 4a) while there were voltage plateaus at around 0.6 and 0.8 V during the initial discharge for cell Li/NiRu–C–NF-2 (Fig. 4b). Subsequent plateaus were located in the range of 1.1–1.3 V during discharge and 2.0–2.25 V during charge, respectively. Furthermore, NiRu–C–NF-2 demonstrated a better stability of keeping electrochemical active plateaus. The galvanostatic profile was in good agreement with the CV results.

Changes in the capacity of the NiRu–C–NF-0 and NiRu–C–NF-2 cells as a function of the cycle number were presented (Fig. 5a). It could be clearly seen that NiRu–C–NF-2 (nickel/ruthenium combined) sample had a better electrochemical performance with high capacity and cyclic stability as opposed to NiRu–C–NF-0 (nickel combined) sample. The measured first discharge capacity of 700 mAh $g^{-1}$ for NiRu–C–NF-0 corresponds to the insertion of $x = 1.95$ mol of Li per formula unit. The first charge (Li-extraction) capacity is 340 mAh $g^{-1}$ and it retained a capacity of 230 mAh $g^{-1}$ at the end of 40th cycle. The irreversible capacity loss between first discharge and charge cycle was 360 mAh $g^{-1}$ and capacity fading from 2 to 40 cycles was 26%. Our observed value which is lower than the theoretical capacity of NiO might be attributed to the presence of electrochemically inactive metallic Ni. For NiRu–C–NF-2, showed an irreversible capacity loss (ICL) of 270 mAh $g^{-1}$ and it retained a stable capacity of 350 mAh $g^{-1}$ up to 40 cycles, which was higher than that of NiRu–C–NF-0 because it contained more active $NiO/RuO_2$. The ICL capacity fade between 2 and 40 cycles is 2.6% and Coulombic efficiency ~98% after 30th cycle. Due to composite nature of our material, it was difficult to compare our capacity values with pure NiO nanomaterials, thin and bulk materials reported in literature. The initial cycle ICL arises due to irreversible consumption of Li for the formation of solid electrolyte interface [4,18,36,37], kinetic limitations [38–40] and other reasons such as intrinsic nature of the material, current density, decomposition of electrolyte followed by formation of the polymeric layer [4].

Rate capability studies for both the materials are shown in Fig. 5b. The obtained capacity value for NiRu–C–NF-0 is ~70 mAh $g^{-1}$ at current rate of 4 C from its initial capacity of 300 mAh $g^{-1}$. NiRu–C–NF-2 showed higher capacity; yet, it faded

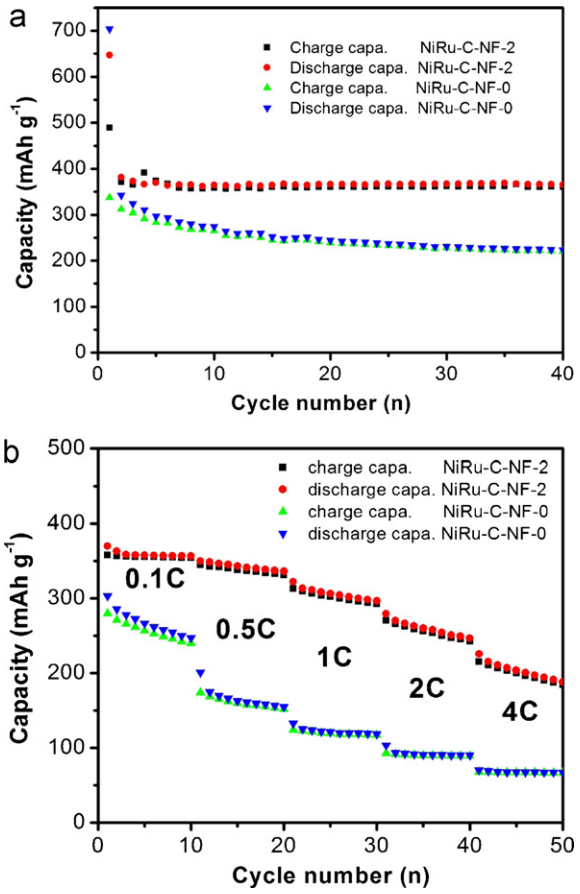


**Fig. 5.** (a)Capacity vs. cycle number plots of cell Li/NiRu–C–NF-0 (5% Ni) and Li/NiRu–C–NF-2 (5% Ni, 15% Ru). Voltage range, 0.005–3.0 V; (a) current rate, 72 mAg$^{-1}$, (b) Rate capability studies taken after 40 cycles running at 0.1 C aged for 2 months (assume 1C = 720 mAg$^{-1}$).

more quickly at higher rates and obtained reversible capacity 185 mAh g$^{-1}$ at 4 C rate. The drop in the capacity at high rates could be attributed to due kinetic limitations and overall NiRu–C–NF-2 composite deliver good rate capability then the NiRu–C–NF-0 composite sample.

### 3.3. Hybrid supercapacitors studies

The galvanostatic cycling performance of the AC/NiRu–C–NF between 0.005 and 3.0 V at a current of 30 mA g$^{-1}$ at room temperature is shown in Fig. 6a. The plot of specific capacitance ($C_{sp}$) vs. cycle number of the corresponding AC/NiRu–C–NF at a current of 30 mA g$^{-1}$ between 0.005 and 3.0 V is shown in Fig. 6b. The capacitance ($C_{cell}$) and $C_{sp}$ were obtained applying the following equation [41] $C_{cell} = (t \times i)/\Delta V$, $C_{sp} = C_{cell}/m$, where $t$ is step time, $i$ is current passing through lithium battery cell, $m$ is the mass of active materials (both composite NF and AC materials) and $\Delta V$ is the potential difference. It can be observed that both NiRu–C–NF-0 and NiRu–C–NF-2 cells share an increase of the specific capacitance after a drop from initial cycles. It is quite interesting and can be analyzed that metallic Ni or Ru might retard active materials (CNF, NiO and $RuO_2$) fully involving during initial electrochemical cycles. After cycling for 30 cycles, the NiRu–C–NF-2 cell has a better charge capacitance of ~60 F g$^{-1}$ in comparison with the NiRu–C–NF-0 cell showed a charge capacitance value of ~30 F g$^{-1}$ in the end of 30th cycle. The better performance for the NiRu–C–NF-2 sample could be attributed to the better electronic conductivity of the Ru composites, which can be seen from the electrochemical

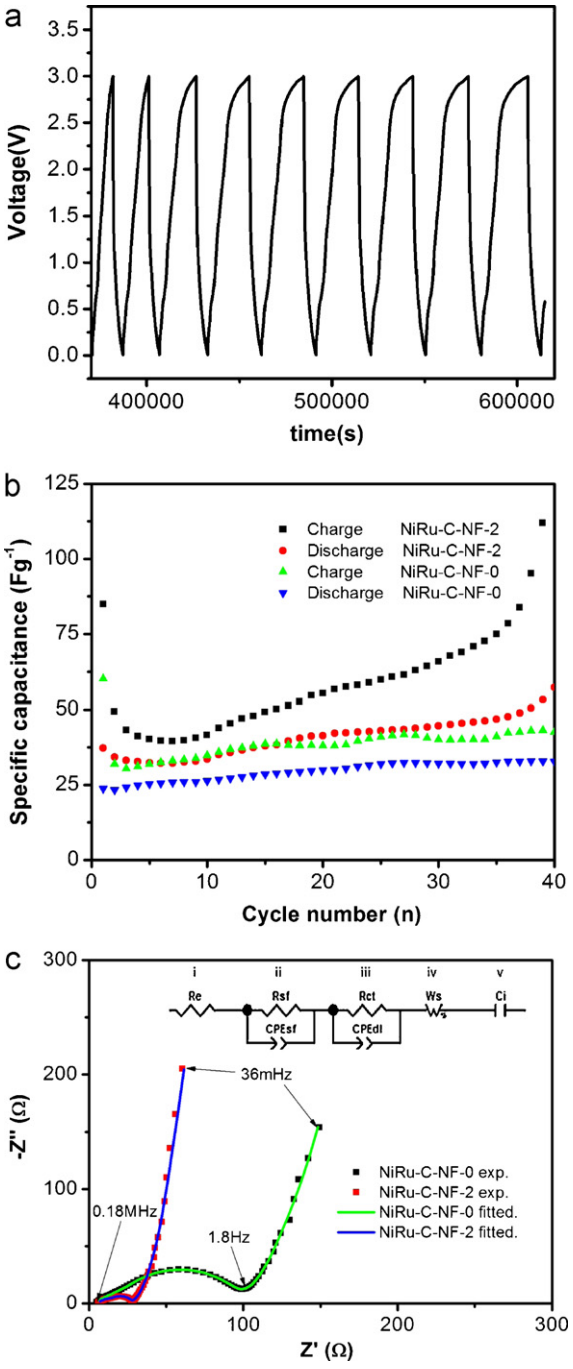


**Fig. 6.** (a) Galvanostatic profiles (voltage vs. time plots) of cell AC/NiRu–C–NF-2 (5% Ni, 15% Ru); (b) plots of specific capacitance ($C_{sp}$) vs. cycle number of cell AC/NiRu–C–NF-0 (5% Ni) and AC/NiRu–C–NF-2 (5% Ni, 15% Ru) at a current of 30 mA g$^{-1}$ between 0.00 and 3.0 V; (c) Nyquist plots ($Z'$ vs. $-Z''$) for two cells in the application of supercapacitor; equivalent circuit used for fitting the experimental data are shown in (c) inset; fitted data are presented in line while experimental data are shown in symbol.

impedance studies and corresponding experimental nyquist plots ($Z'$ and $-Z''$) on fresh cell are shown in Fig. 6c. The experimental spectra was fitted with equivalent electrical circuit composed of five parts, resistance (Ri) (electrolyte (e), surface film (sf) and charge-transfer (ct)), a constant phase element (CPEi) (sf and double layer (dl)) used instead of pure capacitor due to the composite nature of electrode, Warburg impedance (Ws) and intercalation capacitance (Ci), is also presented to fit the experimental impedance data. All fitting data obtained in the frequency

range from 0.18 MHz to 36 mHz. The fitted impedance values for NiRu–C–NF-0, $R_e$, $R_{sf}$ and $R_{ct}$ are 4, 66 (±1) and 23 (±1) Ω, respectively and corresponding values for NiRu–C–NF-2 are 5.5, 10 (±0.5) and 11 (±0.5) Ω. The capacitance values are 95 (±2) μF ($CPE_{sf}$), 223 (±10) μF ($CPE_{dl}$) for NiRu–C–NF-0 and 81 (±2) μF ($CPE_{sf}$), 94 (±2) μF ($CPE_{dl}$) for NiRu–C–NF-2. This can also be applied to confirm the better conductivity and electrode kinetics of Ru composite electrode. The reasons for the increase of capacitance values after 30 cycles in the case of NiRu–C–NF-2 cell are not clear at present. The our present capacitance values of NiRu–C–NF-0 are close to literature studies on $TiP_2O_7$/AC [41] and we observed slightly higher capacitance values with NiRu–C–NF-2, which probably due presence of $Ru/RuO_2$ leads to increased electronic conductivity of the sample and also many reports showed $RuO_2$ based materials showed high capacitance values in aqueous system.

## 4. Conclusions

Thermal assisted electrospinning was applied for the fabrication of Ni/Ru embedded carbon nanofibers. They were characterized by powder X-ray diffraction and Rietveld analysis, SEM and BET measurement. Cyclic voltammetry results of 5 wt% Ni, and 15 wt% Ru embedded CNF showed main peak voltages values at ∼1.25 and ∼2.25 V vs. Li during cathodic and anodic scans, respectively. Li-cycling of NiRu–C–NF-0 and NiRu–C–NF-2 composite samples showed a reversible capacity of 230 and 350 mAh $g^{-1}$ at current rate of 72 mA $g^{-1}$ at the end of 40th cycle. Hybrid supercapacitors made with activated carbon and in non-aqueous electrolyte showed specific discharge capacitance ∼60 F $g^{-1}$ at the end of 30th cycle at a current rate of 30 mA $g^{-1}$.

## Acknowledgments

Authors thank NUS Graduate School for Integrative Sciences and Engineering (NGS) for scholarship, and thanks are due to Prof. G V Subba Rao and Dr. V. Aravindan for helpful discussions.

## References

[1] C. Liu, F. Li, L.P. Ma, H.M. Cheng, Adv. Mater. 22 (2010) E28–E62.
[2] M. Armand, J.M. Tarascon, Nature 451 (2008) 652–657.
[3] P.G. Bruce, B. Scrosati, J.M. Tarascon, Angew. Chem. Int. Ed. 47 (2008) 2930–2946.
[4] M.V. Reddy, G.V. Subba Rao, B.V.R. Chowdari, Binary, ternary and complex metal oxides as anode materials for Li-ion batteries, Chem. Rev, 2011 (under revision).
[5] D.S. Su, R. Schlogl, ChemSusChem 3 (2010) 136–168.
[6] M. Inagaki, H. Konno, O. Tanaike, J. Power Sources 195 (2010) 7880–7903.
[7] J.R. McDonough, J.W. Choi, Y. Yang, F. La Mantia, Y. Cui, Y.G. Zhang, Appl. Phys. Lett. 95 (2009) 243109.
[8] F. Pico, J. Ibanez, M.A. Lillo-Rodenas, A. Linares-Solano, R.M. Rojas, J.M. Amarilla, J.M. Rojo, J. Power Sources 176 (2008) 417–425.
[9] M.S. Wu, J.T. Lee, P.C.J. Chiang, J.C. Lin, J. Mater. Sci. 42 (2007) 259–265.
[10] C. Kim, J. Power Sources 142 (2005) 382–388.
[11] J. Li, E.H. Liu, W. Li, X.Y. Meng, S.T. Tan, J. Alloys Compd. 478 (2009) 371–374.
[12] N. Hedin, V. Sobolev, L.F. Zhang, Z.T. Zhu, H. Fong, J. Mater. Sci. 46 (2011) 6453–6456.
[13] Z.M. Huang, Y.Z. Zhang, M. Kotaki, S. Ramakrishna, Compos. Sci. Technol. 63 (2003) 2223–2253.
[14] V. Thavasi, G. Singh, S. Ramakrishna, Energy Environ. Sci. 1 (2008) 205–221.
[15] M.V. Reddy, R. Jose, T.H. Teng, B.V.R. Chowdari, S. Ramakrishna, Electrochim. Acta 55 (2010) 3109–3117.
[16] P.N. Zhu, Y.Z. Wu, M.V. Reddy, A.S. Nair, B.V.R. Chowdari, S. Ramakrishna, Long term cycling studies of electrospun $TiO_2$ nanostructures and their composites with MWCNTs for rechargeable Li-ion batteries, RSC Adv., 2012, doi:10.1039/C1RA00514F.
[17] A. Le Viet, M.V. Reddy, R. Jose, B.V.R. Chowdari, S. Ramakrishna, J. Phys. Chem. C 114 (2010) 664–671.
[18] P. Poizot, S. Laruelle, S. Grugeon, L. Dupont, J.M. Tarascon, Nature 407 (2000) 496–499.
[19] J. Cabana, L. Monconduit, D. Larcher, M.R. Palacin, Adv. Mater. 22 (2010) E170–E192.
[20] P. Simon, Y. Gogotsi, Nat. Mater. 7 (2008) 845–854.
[21] W.C. Chen, C.C. Hu, C.C. Wang, C.K. Min, J. Power Sources 125 (2004) 292–298.
[22] I.H. Kim, J.H. Kim, Y.H. Lee, K.B. Kim, J. Electrochem. Soc. 152 (2005) A2170–A2178.
[23] Y.W. Ju, G.R. Choi, H.R. Jung, C. Kim, K.S. Yang, W.J. Lee, J. Electrochem. Soc. 154 (2007) A192–A197.
[24] A. Le Viet, M.V. Reddy, R. Jose, B.V.R. Chowdari, S. Ramakrishna, Electrochim. Acta 56 (2011) 1518–1528.
[25] Y.Z. Wu, M.V. Reddy, B.V.R. Chowdari, S. Ramakrishman, Electrochemical studies on electrospun Li(Li1/3Ti5/3)O4 grains as an anode for Li-ion batteries, Electrochim Acta, 2011 (accepted).
[26] M.V. Reddy, G.V. Subba Rao, B.V.R. Chowdari, J. Power Sources 195 (2010) 5768–5774.
[27] E.J. Ra, E. Raymundo-Pinero, Y.H. Lee, F. Beguin, Carbon 47 (2009) 2984–2992.
[28] Y. Wang, S. Serrano, J.J. Santiago-Aviles, Synth. Met. 138 (2003) 423–427.
[29] C. Kim, K.S. Yang, Appl. Phys. Lett. 83 (2003) 1216–1218.
[30] S. Komaba, N. Kumagai, Y. Kataoka, Electrochim. Acta 47 (2002) 1229–1239.
[31] B. Varghese, M.V. Reddy, Z. Yanwu, C.S. Lit, T.C. Hoong, G.V. Subba Rao, B.V.R. Chowdari, A.T.S. Wee, C.T. Lim, C.H. Sow, Chem. Mater. 20 (2008) 3360–3367.
[32] X.F. Li, A. Dhanabalan, K. Bechtold, C.L. Wang, Electrochem. Commun. 12 (2010) 1222–1225.
[33] C. Wang, D.L. Wang, Q.M. Wang, H.J. Chen, J. Power Sources 195 (2010) 7432–7437.
[34] X.H. Wang, Z.B. Yang, X.L. Sun, X.W. Li, D.S. Wang, P. Wang, D.Y. He, J. Mater. Chem. 21 (2011) 9988–9990.
[35] S. Megahed, B. Scrosati, J. Power Sources 51 (1994) 79–104.
[36] S. Grugeon, S. Laruelle, R. Herrera-Urbina, L. Dupont, P. Poizot, J.M. Tarascon, J. Electrochem. Soc. 148 (2001) A285–A292.
[37] P.L. Taberna, S. Mitra, P. Poizot, P. Simon, J.M. Tarascon, Nat. Mater. 5 (2006) 567–573.
[38] M.V. Reddy, T. Yu, C.H. Sow, Z.X. Shen, C.T. Lim, G.V. Subba Rao, B.V.R. Chowdari, Adv. Funct. Mater. 17 (2007) 2792–2799.
[39] M.V. Reddy, S. Madhavi, G.V. Subba Rao, B.V.R. Chowdari, J. Power Sources 162 (2006) 1312–1321.
[40] M.V. Reddy, B. Pecquenard, P. Vinatier, A. Levasseur, Electrochem. Commun. 9 (2007) 409–415.
[41] V. Aravindan, M.V. Reddy, S. Madhavi, S.G. Mhaisalkar, G.V. Subba Rao, B.V.R. Chowdari, J. Power Sources 196 (2011) 8850–8854.